

Galaxy clustering constraints on deviations from Newtonian gravity at cosmological scales II: Perturbative and numerical analyses of power spectrum and bispectrum

Akihito Shirata^(1,2), Yasushi Suto^(2,3), Chiaki Hikage⁽⁴⁾ * , Tetsuya Shiromizu⁽¹⁾, Naoki Yoshida⁽⁴⁾

⁽¹⁾*Department of Physics, Tokyo Institute of Technology, Tokyo 152-8551, Japan*

⁽²⁾*Department of Physics, The University of Tokyo, Tokyo 113-0033, Japan*

⁽³⁾*Research Center for the Early Universe, The University of Tokyo, Tokyo 113-0033, Japan and*

⁽⁴⁾*Department of Physics, Nagoya University, Nagoya 464-8602, Japan*

(Dated: November 15, 2018)

We explore observational constraints on possible deviations from Newtonian gravity by means of large-scale clustering of galaxies. We measure the power spectrum and the bispectrum of Sloan Digital Sky Survey galaxies and compare the result with predictions in an empirical model of modified gravity. Our model assumes an additional Yukawa-like term with two parameters that characterize the amplitude and the length scale of the modified gravity. The model predictions are calculated using two methods; the second-order perturbation theory and direct N -body simulations. These methods allow us to study non-linear evolution of large-scale structure. Using the simulation results, we find that perturbation theory provides reliable estimates for the power spectrum and the bispectrum in the modified Newtonian model. We also construct mock galaxy catalogues from the simulations, and derive constraints on the amplitude and the length scale of deviations from Newtonian gravity. The resulting constraints from power spectrum are consistent with those obtained in our earlier work, indicating the validity of the previous empirical modeling of gravitational nonlinearity in the modified Newtonian model. If linear biasing is adopted, the bispectrum of the SDSS galaxies yields constraints very similar to those from the power spectrum. If we allow for the nonlinear biasing instead, we find that the ratio of the quadratic to linear biasing coefficients, b_2/b_1 , should satisfy $-0.4 < b_2/b_1 < 0.3$ in the modified Newtonian model.

PACS numbers: 04.50.+h 98.65.-r 98.80.Es

I. INTRODUCTION

Recent measurements of cosmic microwave background radiation angular power spectrum [1, 2, 3] strongly support the “standard” cosmological model in which the energy content of the universe is dominated by dark energy (very close to Einstein’s cosmological constant, Λ) and cold dark matter (CDM). Such Λ CDM universes are also in good agreement with independent datasets of galaxy clustering [4, 5] and distant Type Ia supernovae [6, 7, 8]. Thus the basic framework for the theory of structure formation in the universe is firmly established. Nevertheless the nature and the physical origin of dark energy remain to be understood.

The apparent accelerating expansion of the universe is conventionally interpreted in terms of a source of repulsive force (dark energy), but can be explained by modifying Newton’s law of gravity on cosmological scales as well. The latter resolution has been seriously considered recently. For example, Dvali, Gabadadze and Porrati (DGP) [9, 10] propose that gravity leaking into extra dimensions drives the observed accelerating expansion. Other such models include modified Newtonian dynamics (MOND) [11, 12, 13] and ghost condensation [14, 15]. Intriguingly, *all* of these alternative models predict some

deviation from conventional Newtonian gravity at cosmological scales.

Indeed, while the validity of Newtonian gravity is tested to high precision up to the scale of the solar system ($\sim 10^{13}$ m), there have been no rigorous tests at sub-millimeter and over scales beyond the solar system [16, 17, 18]. It has been suggested that large-scale galaxy clustering can be used to constrain non-Newtonian models of gravity [19] in principle, but it became feasible only recently with accurate measurements of galaxy clustering in large redshift surveys [4, 5].

In our earlier work [20] (Paper I), we put quantitative constraints on deviations from Newtonian gravity at cosmological scales under the assumption that the deviation can be described in a simple parametric form; we adopted an empirical Yukawa-like term for the modified gravity, and calculated the galaxy-galaxy power spectrum semi-analytically. (See also Ref. [21] for similar argument.) By comparing the predicted power spectrum with that of SDSS galaxies [4], we derived quantitative, although still conditional, constraints on deviations from Newton’s law of gravity.

In this paper, we improve our previous work by performing non-linear cosmological simulations and by exploiting a higher-order statistic, bispectrum. Since bispectrum is sensitive to clustering in the non-linear regime, it is expected to provide complementary constraints at mega-parsec scales to that obtained from power spectrum analysis. We use direct N -body simulations to test the accuracy of our semi-analytic calculations and to reinforce our conclusions.

*Present address: School of Physics and Astronomy, University of Nottingham, University Park, Nottingham NG7 2RD, United Kingdom

The rest of the paper is organized as follows. Our model assumptions are described in Sec. II. We derive power spectrum and bispectrum from perturbation theory in modified Newtonian model in Sec. III and IV. We perform N -body simulations and construct mock samples of volume-limited SDSS galaxies for direct comparison with the observational data. Details of the simulations are described in Sec. V. The results of perturbation theory and the simulations are discussed in Sec. VI and VII. Finally Sec. VIII concludes the present analysis.

II. MODEL ASSUMPTIONS

In this section, we briefly summarize our model and a set of assumptions. Further details may be found in Paper I.

We consider a modified Newtonian model for which gravitational potential is given by

$$\Phi(\mathbf{r}) = -G_N \int dr'^3 \frac{\rho(\mathbf{r}')}{|\mathbf{r} - \mathbf{r}'|} \left[1 + \alpha \left(1 - e^{-\frac{|\mathbf{r} - \mathbf{r}'|}{\lambda}} \right) \right], \quad (1)$$

where G_N denotes (conventional) Newton's constant of gravity. The above model corresponds to Model II in Paper I, on which we focus throughout the following analysis. The deviation from the Newtonian gravity in this model is characterized by two parameters, α and λ ; α is the dimensionless amplitude of the deviation and λ is the characteristic length scale. Note that λ is defined in the proper length, rather than in the comoving length.

It is important to note that, although we consider deviations from Newtonian gravity at mega-parsec scales, we still assume that the global cosmic expansion is unaffected by the deviations. Namely, we assume that general relativity is valid on horizon scales and thus the cosmic expansion is described by the standard Friedmann equation. Strictly speaking, these two assumptions may be in conflict with modified gravity models in general [22, 23, 24, 25, 26]. To account for the existing data such as SNeIa and CMB, however, the cosmic expansion law can hardly change in practice. This is why we adopt the conventional Friedmann equation even in this analysis. For the same reason, we use conventional matter transfer function as initial condition of dark matter adopting the background cosmology defined by the standard set of cosmological parameters, $\Omega_m=0.3$, $\Omega_b=0.04$, $\Omega_\Lambda = 0.7$, and the Hubble constant at present $h = 0.7$ in units of $100\text{km s}^{-1} \text{Mpc}^{-1}$. See Paper I for further discussion on this point.

In order to make a direct comparison between the clustering of SDSS galaxies and our model predictions, we need to assume a biasing relation for the distribution of galaxies and that of matter. For this purpose, we adopt a commonly adopted deterministic relation:

$$\delta_{\mathbf{k}, \text{galaxy}} = b_1 \delta_{\mathbf{k}} + \frac{b_2}{2} \delta_{\mathbf{k}}^2, \quad (2)$$

where $\delta_{\mathbf{k}, \text{galaxy}}$ and $\delta_{\mathbf{k}}$ are fractional fluctuation of galaxy number and mass density, b_1 and b_2 are linear and quadratic biasing parameters. We consider only linear bias (i.e., $b_2 = 0$) when we use power spectrum, whereas we consider both b_1 and b_2 for analyses using bispectrum. To derive constraints on α and λ , b_1 is treated as a free parameter to adjust the overall clustering amplitude.

III. POWER SPECTRUM ANALYSIS

In Fourier space, the modified gravitational potential in Eq. (1) can be written as

$$[\Delta_{\mathbf{x}} \Phi(\mathbf{x})]_{\mathbf{k}} = 4\pi G_N a^2 \bar{\rho} \left[1 + \alpha \frac{\left(\frac{a}{k\lambda}\right)^2}{1 + \left(\frac{a}{k\lambda}\right)^2} \right] \delta_{\mathbf{k}}, \quad (3)$$

where \mathbf{x} is in the comoving coordinate, \mathbf{k} is the comoving wave-number, and a is the scale factor normalized unity at the present epoch.

For the potential of Eq. (3), the evolution equation for density perturbations is written as

$$\mathcal{D}_k \delta_{\mathbf{k}}^{(1)} = 0, \quad (4)$$

with

$$\mathcal{D}_k \equiv \frac{d^2}{dt^2} + 2H(a) \frac{d}{dt} - \mathcal{H}_k, \quad (5)$$

$$\mathcal{H}_k \equiv \frac{3}{2} H^2(a) \Omega_m(a) \left[1 + \alpha \frac{\left(\frac{a}{k\lambda}\right)^2}{1 + \left(\frac{a}{k\lambda}\right)^2} \right], \quad (6)$$

where $H(a)$ is the Hubble parameter, and $\delta_{\mathbf{k}}^{(1)}$ denotes the linear term in density fluctuations [see Eq. (16) below]. Note that even the linear perturbation equation becomes dependent on k in the modified gravity model.

Next, the linear power spectrum $P_L(k)$ at present is given by

$$P_L(k; \alpha, \lambda) = AT^2(k) k^n \left[\delta_{\mathbf{k}}^{(1)}(a = 1; \alpha, \lambda) \right]^2, \quad (7)$$

where $T(k)$ is the matter transfer function, and n is the spectral index of the primordial power spectrum which we set to be unity. We use the fitting formula of Eisenstein and Hu [27] for $T(k)$. It should be emphasized here that we fix the amplitude A so that the rms value of the top-hat mass fluctuations at $8h^{-1}\text{Mpc}$, σ_8 , equals 0.9 **when $\alpha = 0$ and $n = 1$** . The actual value of σ_8 in our modified gravity model may be slightly different because of the factor $\left[\delta_{\mathbf{k}}^{(1)}(a = 1; \alpha, \lambda) \right]^2$ in Eq. (7). However, the difference in the overall amplitude is unimportant because we have an additional freedom to adjust the predicted amplitude via the biasing relation [Eq. (2)].

In Paper I we used the Peacock-Dodds prescription [28] to convert the linear power spectrum to nonlinear one. It turned out that in doing so we used incorrectly

the growth factor $g(\Omega)$ and the tilt of linear power spectrum $n_L(k_L)$ given in the case of Newtonian models. We made sure later that the above mistake did not change the final power spectra very much as long as the Peacock-Dodds prescription is valid. In the present paper, we also confirm the validity of the Peacock-Dodds approach in non-Newtonian models using N -body simulations directly (see Sec. VI).

IV. PERTURBATION THEORY AND BISPECTRUM

In this section, we describe the second order perturbation theory and its application to bispectrum. The earlier formulation of cosmological perturbation in the Newtonian model may be found in [29, 30, 31, 32]. Bernardeau [33] developed a formulation of second order perturbation theory in non-Newtonian models. We apply the method to the modified potential in Eq. (1).

The basic equations are given by

$$\dot{\delta} + \frac{1}{a}\partial_i \{v^i (1 + \delta)\} = 0, \quad (8)$$

$$\dot{v}^i + \frac{1}{a}v^j \partial_j v^i + \frac{\dot{a}}{a}v^i = -\frac{1}{a}\partial_i \Phi, \quad (9)$$

where the over-dot denotes the derivative with respect to time, $v^i (= a\dot{x}^i)$ is the peculiar velocity, and Φ is the gravitational potential. We define velocity divergence:

$$u(\mathbf{x}, t) \equiv \partial_i v^i(\mathbf{x}, t). \quad (10)$$

Equations (8) and (9) in Fourier space reduce to

$$a\dot{\delta}_{\mathbf{k}} + u_{\mathbf{k}} = -\frac{1}{2(2\pi)^3} \int d^3p [F(\mathbf{k}, \mathbf{p})u_{\mathbf{p}}\delta_{\mathbf{q}} + F(\mathbf{k}, \mathbf{q})u_{\mathbf{q}}\delta_{\mathbf{p}}] \quad (11)$$

$$F(\mathbf{k}, \mathbf{p}) \equiv \frac{\mathbf{k} \cdot \mathbf{p}}{p^2}, \quad (12)$$

$$\mathbf{q} \equiv \mathbf{k} - \mathbf{p}, \quad (13)$$

and

$$\dot{u}_{\mathbf{k}} + Hu_{\mathbf{k}} + a\mathcal{H}_k\delta_{\mathbf{k}} = -\frac{1}{(2\pi)^3 a} \int d^3p G(\mathbf{k}, \mathbf{p}, \mathbf{q})u_{\mathbf{p}}u_{\mathbf{q}}, \quad (14)$$

$$G(\mathbf{k}, \mathbf{p}, \mathbf{q}) \equiv \frac{k^2}{2p^2} \frac{\mathbf{p} \cdot \mathbf{q}}{q^2}. \quad (15)$$

These equations can be solved recursively. Let us first decompose $\delta_{\mathbf{k}}$ and $u_{\mathbf{k}}$ perturbatively,

$$\delta_{\mathbf{k}} = \delta_{\mathbf{k}}^{(1)} + \delta_{\mathbf{k}}^{(2)} + \delta_{\mathbf{k}}^{(3)} + \dots, \quad (16)$$

$$u_{\mathbf{k}} = u_{\mathbf{k}}^{(1)} + u_{\mathbf{k}}^{(2)} + u_{\mathbf{k}}^{(3)} + \dots. \quad (17)$$

Differentiating Eq. (11) and substituting to Eq. (14) to eliminate $u_{\mathbf{k}}$, we obtain

$$\mathcal{D}_k \delta_{\mathbf{k}}^{(n)} = \frac{\dot{A}^{(n)}}{a} + \frac{H}{a}A^{(n)} - \frac{B^{(n)}}{a}, \quad (18)$$

where $A^{(n)}$ and $B^{(n)}$ are the source terms of the n th-order:

$$A^{(n)} \equiv -\frac{1}{2(2\pi)^3} \int d^3p \left[F(\mathbf{k}, \mathbf{p}) \sum_{i=1}^{n-1} u_{\mathbf{p}}^{(i)} \delta_{\mathbf{q}}^{(n-i)} + (\mathbf{p} \leftrightarrow \mathbf{q}) \right], \quad (19)$$

$$B^{(n)} \equiv -\frac{1}{(2\pi)^3 a} \int d^3p \left[G(\mathbf{k}, \mathbf{p}, \mathbf{q}) \sum_{i=1}^{n-1} u_{\mathbf{p}}^{(i)} u_{\mathbf{q}}^{(n-i)} \right]. \quad (20)$$

Consider first the lowest order, $n = 1$. Since $A^{(1)} = B^{(1)} = 0$, Eq. (18) reduces to

$$\mathcal{D}_k \delta_{\mathbf{k}}^{(1)} = 0, \quad (21)$$

which is equivalent to Eq. (4). We denote the growing mode of the solution of Eq. (21) by $D_k^{(1)}(t)$. Note that, in non-Newtonian models, the solution $D_k^{(1)}(t)$ is generally dependent on scale k , in contrast to the conventional Newtonian case. The linear solution $\delta_{\mathbf{k}}^{(1)}$ is given by

$$\delta_{\mathbf{k}}^{(1)} = D_k^{(1)} \delta_{\text{ini}}(\mathbf{k}), \quad (22)$$

where $\delta_{\text{ini}}(\mathbf{k})$ is the initial fractional density.

The corresponding linear solution for $u_{\mathbf{k}}$ is obtained from Eq. (11) as

$$u_{\mathbf{k}}^{(1)} = -a\dot{\delta}_{\mathbf{k}}^{(1)} = -a\dot{D}_k^{(1)} \delta_{\text{ini}}(\mathbf{k}). \quad (23)$$

Solutions at the next order, $n = 2$, are more complicated. Eq. (18) for $n = 2$ is written explicitly as

$$\mathcal{D}_k \delta_{\mathbf{k}}^{(2)} = \frac{1}{(2\pi)^3} \int d^3 p d^3 q \delta^D(\mathbf{p} + \mathbf{q} - \mathbf{k}) \{ \delta_{\text{ini}}(\mathbf{p}) \delta_{\text{ini}}(\mathbf{q}) [S_0(p, q, t) \mathcal{P}_0(\mu) + S_1(p, q, t) \mathcal{P}_1(\mu) + S_2(p, q, t) \mathcal{P}_2(\mu)] \}, \quad (24)$$

$$S_0(p, q, t) = \left(\frac{\mathcal{H}_p}{2} + \frac{\mathcal{H}_q}{2} \right) D_p^{(1)} D_q^{(1)} + \frac{4}{3} \dot{D}_p^{(1)} \dot{D}_q^{(1)}, \quad (25)$$

$$S_1(p, q, t) = \left(\frac{\mathcal{H}_p}{2} \frac{q}{p} + \frac{\mathcal{H}_q}{2} \frac{p}{q} \right) D_p^{(1)} D_q^{(1)} + \left(\frac{q}{p} + \frac{p}{q} \right) \dot{D}_p^{(1)} \dot{D}_q^{(1)}, \quad (26)$$

$$S_2(p, q, t) = \frac{2}{3} \dot{D}_p^{(1)} \dot{D}_q^{(1)}, \quad (27)$$

where $\delta^D(\mathbf{k})$ is the Delta function and $\mathcal{P}_l(\mu)$ are the Legendre polynomials:

$$\mathcal{P}_0(\mu) = 1, \quad \mathcal{P}_1(\mu) = \mu, \quad \mathcal{P}_2(\mu) = \frac{1}{2} (3\mu^2 - 1), \quad (28)$$

$$\mu \equiv \frac{\mathbf{p} \cdot \mathbf{q}}{pq}. \quad (29)$$

Equation (24) has an implicit solution of the form:

$$\delta_{\mathbf{k}}^{(2)} = \frac{1}{(2\pi)^3} \int d^3 p d^3 q \delta^D(\mathbf{p} + \mathbf{q} - \mathbf{k}) [\delta_{\text{ini}}(\mathbf{p}) \delta_{\text{ini}}(\mathbf{q}) \times \{T_0(p, q, t) \mathcal{P}_0(\mu) + T_1(p, q, t) \mathcal{P}_1(\mu) + T_2(p, q, t) \mathcal{P}_2(\mu)\}], \quad (30)$$

where the functions $T_i(p, q, t)$ satisfy

$$\mathcal{D}_{|\mathbf{p}+\mathbf{q}|} T_i(p, q, t) = S_i(p, q, t) \quad \text{for } i = 0, 1, 2. \quad (31)$$

We note that expressions for the second-order solutions given in [33] contain some typographical errors which are corrected in our above expressions.

These results enable us to compute the bispectrum in the leading order. The bispectrum is defined as

$$\langle \delta(\mathbf{k}_1) \delta(\mathbf{k}_2) \delta(\mathbf{k}_3) \rangle = (2\pi)^3 B(\mathbf{k}_1, \mathbf{k}_2, \mathbf{k}_3) \delta^D(\mathbf{k}_1 + \mathbf{k}_2 + \mathbf{k}_3). \quad (32)$$

The leading-order terms of the left-hand-side of the above equation are given by

$$\langle \delta(\mathbf{k}_1) \delta(\mathbf{k}_2) \delta(\mathbf{k}_3) \rangle = \langle \delta^{(2)}(\mathbf{k}_1) \delta^{(1)}(\mathbf{k}_2) \delta^{(1)}(\mathbf{k}_3) \rangle + \text{cyc.}(1, 2, 3). \quad (33)$$

Therefore the bispectrum reduces to

$$B(\mathbf{k}_1, \mathbf{k}_2, \mathbf{k}_3) = 2D_{k_1}^{(1)} D_{k_2}^{(1)} \left[\sum_{i=0}^2 T_i(k_1, k_2, t) \mathcal{P}_i(\mathbf{k}_1, \mathbf{k}_2) \right] \times P_{\text{ini}}(k_1) P_{\text{ini}}(k_2) + \text{cyc.}(1, 2, 3), \quad (34)$$

where $P_{\text{ini}}(k) \equiv \langle |\delta_{\text{ini}}(\mathbf{k})|^2 \rangle$. In what follows, we write the bispectrum simply as $B(\mathbf{k}_1, \mathbf{k}_2)$ adopting the condition of $\mathbf{k}_3 = -\mathbf{k}_2 - \mathbf{k}_1$ [Eq. (32)].

To compute the bispectrum, we solve Eq. (31) numerically for each pair of (\mathbf{p}, \mathbf{q}) , together with the linear perturbation equation (21). At sufficiently early epochs

($z_i \gg 1$), $D_k^{(1)}(z_i)$ is simply given by the growth rate in the Newtonian case (see Paper I). Similarly, T_i are given by

$$T_0(p, q, z_i) = \frac{17}{21} (1 + z_i)^{-2}, \quad (35)$$

$$T_1(p, q, z_i) = \frac{1}{2} \left(\frac{q}{p} + \frac{p}{q} \right) (1 + z_i)^{-2}, \quad (36)$$

$$T_2(p, q, z_i) = \frac{4}{21} (1 + z_i)^{-2}. \quad (37)$$

V. SIMULATION AND OBSERVATIONAL DATA

A. N-body Simulations

We use the cosmological N -body solver TPM-1.1 [34] in its PM-only mode. We run six realizations each for simulation box-sizes of $L_{\text{box}} = 500h^{-1}\text{Mpc}$, and $1000h^{-1}\text{Mpc}$ with the following parameters: $\alpha = -1.0, -0.8, -0.5, -0.2, 0.0, 0.2, 0.5, 0.8$, and 1.0 , $\lambda = 2, 5, 8, 10, 12, 15, 20$, and $30h^{-1}\text{Mpc}$. We use the fitting formula for the matter transfer function, equation (28) \sim (31) of the ref. [27], that ignores the baryon acoustic oscillation effect. We start the simulations at $z = 50$. All the simulations employ $N_p = 128^3$ particles.

To simulate structure formation in the non-Newtonian model, we need to modify the Green function of the Laplacian, $\hat{\mathcal{G}}$. For a density field $\hat{\rho}$ defined on a three-dimensional wave-number grid (p, q, r) , the gravitational potential in real space is evaluated to be

$$\phi(l, m, n) = \sum_{p, q, r=0}^{M-1} \hat{\mathcal{G}}_{p, q, r} \hat{\rho}_{p, q, r} \exp[2\pi i(pl + qm + rn)/M], \quad (38)$$

where l, m, n are position integers in real space with M being the number of grids per dimension (we follow the notation in Efsthathiou *et al.* [35]).

The Green function in the original TPM code that as-

sumes the conventional Newtonian gravity is given by

$$\hat{\mathcal{G}}_{p,q,r}^{\text{old}} = \begin{cases} 0, & l = m = n = 0; \\ -\pi / \{M^2 [\sin^2(\pi p/M) \\ + \sin^2(\pi q/M) + \sin^2(\pi r/M)]\} & \text{otherwise;} \end{cases} \quad (39)$$

which is derived from the seven-point finite-difference approximation.

Taking account of the scale-dependence in Eq. (3), we correct the Green function for the modified Newtonian model:

$$\hat{\mathcal{G}}_{p,q,r}^{\text{new}} = \hat{\mathcal{G}}_{p,q,r}^{\text{old}} \times \left[1 + \alpha \frac{(\frac{a}{k\lambda})^2}{1 + (\frac{a}{k\lambda})^2} \right]. \quad (40)$$

Note that k in Eq. (40) needs to be given in the form, consistently with the Green function itself, as

$$k(p, q, r) = \frac{M}{\pi} \left\{ [\sin^2(\pi p/M) + \sin^2(\pi q/M) + \sin^2(\pi r/M)] \right\}^{1/2} \times \frac{2\pi}{L_{\text{box}}}. \quad (41)$$

We use the above Green function, evolve the system from $z = 50$ to 0, and make mock galaxy samples in the manner described in the next subsection.

B. Observational data and mock samples

For definiteness, we choose a volume-limited sample of SDSS galaxies whose r -band magnitude is in the range of (-21.0, -20.0) from those described in Hikage *et al.* [36]. The redshift range is $0.044 < z < 0.103$, the survey volume, V_{samp} , is $9.20 \times 10^6 (h^{-1}\text{Mpc})^3$, and the total number of galaxies is 44,636. We made sure that using the other volume-limited samples with different magnitude ranges [36] does not significantly affect the results of our analysis below.

We generate 24 mock catalogues from our N -body simulation data. The mock catalogues take into account various observational effects such as survey geometry, the number density, and redshift distortion (peculiar velocities of simulation particles are assigned to the mock galaxies) [36]. In order to account for the effect of survey geometry, we distribute random particles within the survey volume and correct for the boundary effect following the prescription of Feldman, Kaiser and Peacock [37]. We subtract fluctuations of the random particles which are within the survey volume, $\delta_{\mathbf{k},\text{random}}$:

$$\tilde{\delta}_{\mathbf{k}} = \delta_{\mathbf{k},\text{data}} - \delta_{\mathbf{k},\text{random}}. \quad (42)$$

While this prescription is fairly empirical and may not completely account for the effect of the survey geometry, it yields a robust estimate at scales of our main interest here, $k \sim 0.1h\text{Mpc}^{-1}$. When we calculate the power spectrum and bispectrum for SDSS galaxies and the mock catalogues, we use the above ‘‘corrected’’ density, $\tilde{\delta}_{\mathbf{k}}$.

VI. CONSTRAINTS FROM POWER SPECTRUM

We first compare the power spectra used the Peacock-Dodds prescription and those from numerical simulations. In Fig. 1, we plot the mass power spectra in real space (left panels) and in redshift space (right panels). The predictions from perturbation theory agree well with the results of N -body simulations. Note that in the Newtonian case, the predicted power spectra with $b_1 = 1$ are already in reasonable agreement with the observed power spectrum of SDSS galaxies. Our simulation results are also consistent with those of Stabenau and Jain [38].

The panels on the right side in Fig. 1 show the power spectra of our mock ‘‘galaxies’’. In each panel, the dotted line indicates the non-linear power spectrum in real space, which is the same in the corresponding left panel and shown for comparison. The redshift-space power spectrum of the SDSS volume-limited sample is shown by cross symbols. To include effects of redshift space distortion in our model, we use the formula derived of Magira, Jing and Suto [39] [equation (12) in their paper]. On linear scales ($k < 0.1h\text{Mpc}^{-1}$), the Kaiser effect is clearly seen as an enhanced power with respect to the real space power spectrum. It is worth mentioning that the plotted power spectra show substantial variations on the largest scales ($k < 0.03h\text{Mpc}^{-1}$), which are presumably due to the somewhat complex survey geometry.

To derive constraints on α, λ using the calculated power spectra, we apply the $\Delta\chi^2$ statistic. We treat the linear bias parameter b_1 as a free parameter in order to adjust the overall amplitudes of the power spectra between the predictions/simulations and the SDSS data. This normalization allows us to use the *shape* of the power spectra to detect possible deviations from the Newtonian case.

We calculate χ^2 as

$$\chi^2 \equiv \sum_i \frac{[P(k_i) - P_{\text{SDSS}}(k_i)]^2}{\sigma^2(k_i)}, \quad (43)$$

where $P_{\text{SDSS}}(k_i)$ is the SDSS galaxy power spectrum. We use the predicted power spectra $P(k_i)$ and the variance of the SDSS data, $\sigma^2(k_i)$, to calculate χ^2 in real space, while for the same analysis in redshift space, we use those power spectra with the variance of mock galaxy samples to represent the cosmic variance in redshift space.

We compute the relative confidence level of α and λ with respect to their best-fit values assuming that

$$\Delta\chi^2(\alpha, \lambda) \equiv \chi^2(\alpha, \lambda, b_{*,\text{local min}}) - \chi^2(\alpha_{\text{min}}, \lambda_{\text{min}}, b_{*,\text{min}}) \quad (44)$$

follows the χ^2 distribution for 2 degrees of freedom. In Eq. (44), α_{min} , λ_{min} and $b_{*,\text{min}}$ denote their best-fit values which globally minimize the value of χ^2 , while $b_{*,\text{local min}}$ is the value that minimizes the χ^2 for a given set of values of α and λ .

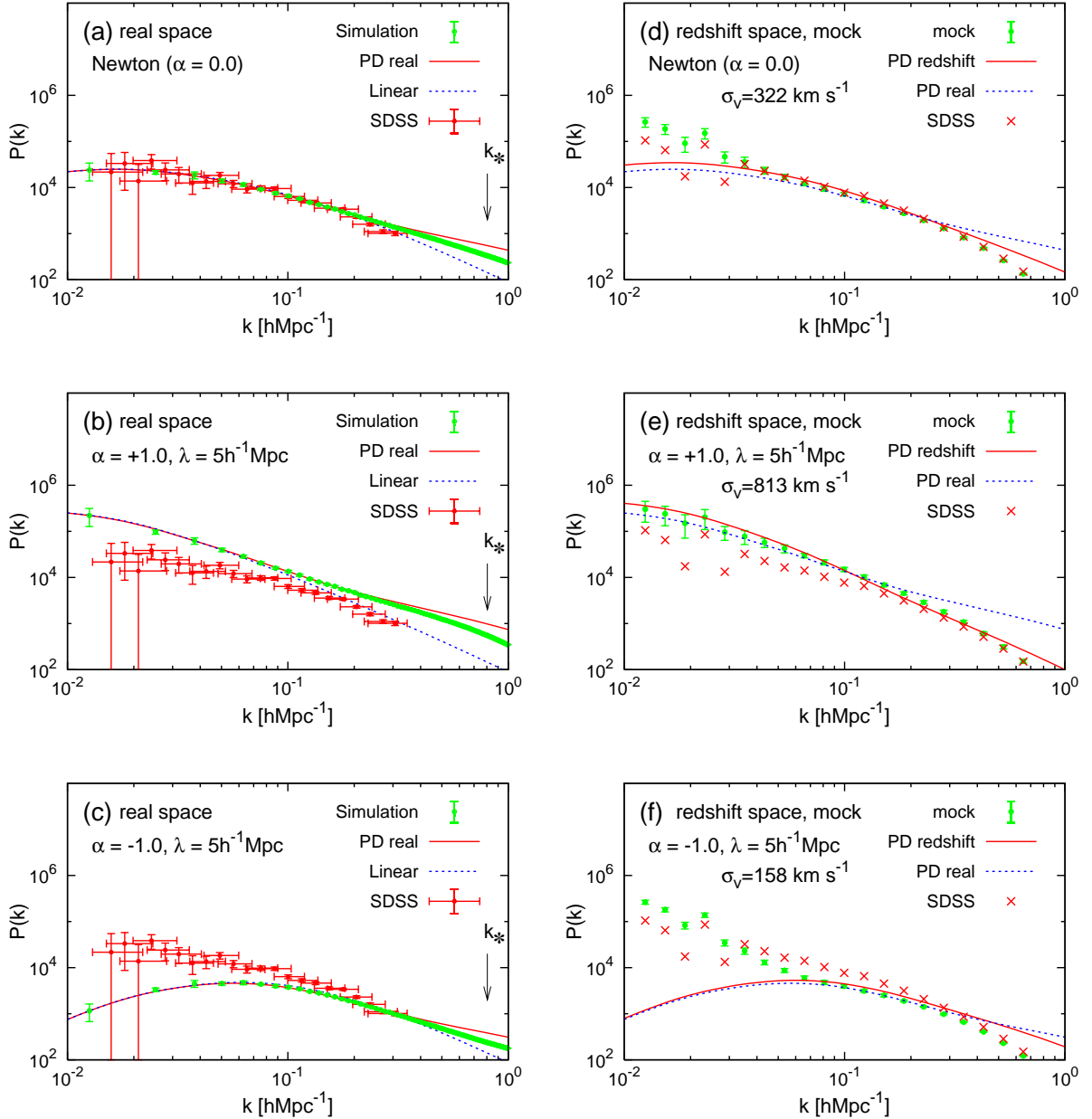


FIG. 1: The panels of the left side show the power spectra in real space. The adopted model parameters are (a) Newtonian ($\alpha = 0.0$), (b) $\alpha = +1.0$ and $\lambda = 5h^{-1}\text{Mpc}$, (c) $\alpha = -1.0$ and $\lambda = 5h^{-1}\text{Mpc}$. Dots with vertical and horizontal error-bars are the power spectrum of SDSS galaxies from Tegmark *et al.* [4]. Dots with only vertical error-bars indicate results of N-body simulations. Dotted and solid lines are linear and non-linear power spectrum, respectively. We denote by k_* the length scale of the mean inter-particle separation in our simulations, which is given by $k_* = 0.5 \cdot 2\pi \cdot N_p^{1/3} / L_{\text{box}}$. The simulation results are reliable at $k < k_*$. In the right panels, we plot the power spectra for mock “galaxies” generated from our simulation. The parameters for (d), (e), (f) are the same as for (a), (b), (c), respectively. The dotted and solid lines in the right panels are non-linear power spectrum in real space (, which are the same as solid lines in the left panels) and redshift space. σ_v means the one-dimensional velocity dispersion calculated from simulation data. Cross symbols are the power spectra of the volume-limited sample of SDSS galaxies

Figure 2 shows the contours of $\Delta\chi^2(\alpha, \lambda)$. The results from N-body simulations in real space are shown in panel (a) and (b). These differ only in the simulation box size, $500 h^{-1}\text{Mpc}$ for (a) and $1000 h^{-1}\text{Mpc}$ for (b). Hence the

range of k used to derive constraints is slightly different, We also show the result from the real-space Peacock-Dodds prediction by thin dotted lines using the the same range of k consistently with the simulations. Clearly, the

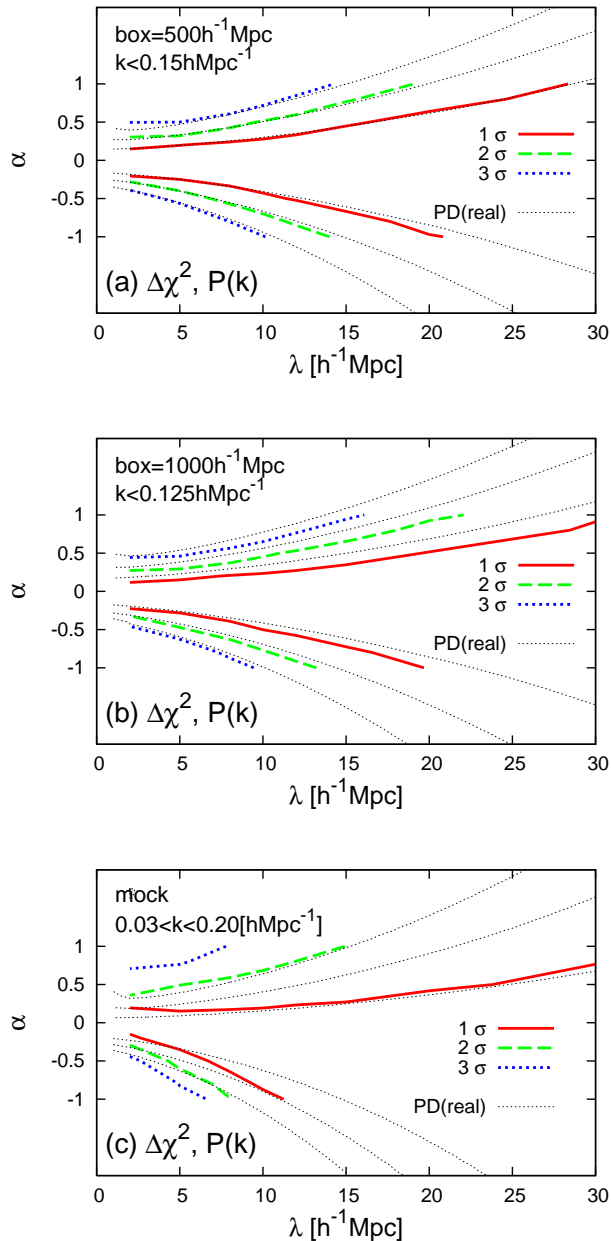


FIG. 2: Constraints on α and λ obtained using (a) simulations with $L_{\text{box}} = 500h^{-1}\text{Mpc}$, (b) simulations with $L_{\text{box}} = 1000h^{-1}\text{Mpc}$, and (c) mock galaxy catalogues. The range of k used to compute χ^2 is indicated in each panel. Thick solid, dotted, thick dotted lines indicate the limits at 1σ , 2σ and 3σ confidence levels. For comparison, we plot the corresponding 1σ , 2σ and 3σ confidence levels using the real-space Peacock-Dodds prediction in thin dotted lines.

results of the perturbation theory and that of our numerical simulations are consistent with each other, putting quite similar constraints on α and λ .

The bottom panel (c) in Figure 2 shows the constraints from our mock galaxy samples in redshift space. The range of k used in the analysis is $0.03 < k < 0.20h\text{Mpc}^{-1}$.

The constraint is slightly less tight than those from perturbation theory and N -body simulations. This is mainly because we discard the data points at large scales $k \sim 0.01h\text{Mpc}^{-1}$ where the deviations from the Newtonian case are most significant. Nevertheless models with $|\alpha| > 1$ are still excluded at a 2-3 σ confidence level for $\lambda \sim 10h^{-1}\text{Mpc}$. For reference, we also plot the contours based on the real-space Peacock-Dodds prediction by thin dotted lines.

VII. CONSTRAINTS FROM BISPECTRUM

We further derive constraints on the modified Newtonian model extending the analysis to the three-point statistics. Specifically we use (conventional) bispectrum, $B(\mathbf{k}_1, \mathbf{k}_2)$, defined in Eq. (32), and reduced bispectra Q and $p^{(3)}$ defined as

$$Q(\mathbf{k}_1, \mathbf{k}_2) = \frac{B(\mathbf{k}_1, \mathbf{k}_2)}{P(k_1)P(k_2) + P(k_2)P(k_3) + P(k_3)P(k_1)}, \quad (45)$$

and

$$p^{(3)}(\mathbf{k}_1, \mathbf{k}_2) = \frac{B(\mathbf{k}_1, \mathbf{k}_2)}{\sqrt{V_{\text{samp}}P(k_1)P(k_2)P(k_3)}}, \quad (46)$$

where $\mathbf{k}_3 \equiv -\mathbf{k}_1 - \mathbf{k}_2$, $k_i = |\mathbf{k}_i|$, and V_{samp} is the sampling volume. The latter quantity $p^{(3)}$ is the probability density function of phase sum for a density field, $\theta_{\mathbf{k}_1} + \theta_{\mathbf{k}_2} + \theta_{\mathbf{k}_3}$ [$\delta_{\mathbf{k}} = |\delta_{\mathbf{k}}| \exp(i\theta_{\mathbf{k}})$], studied in Matsubara [40] and Hikage *et al.* [36, 41]. In this paper, we consider only isosceles triangles in k -space that satisfy the relation $k \equiv k_1 = k_2$ with angle φ defined as

$$\varphi = \cos^{-1} \left(\frac{\mathbf{k}_1 \cdot \mathbf{k}_2}{k_1 k_2} \right). \quad (47)$$

In the following analysis, we use $p^{(3)}$ to give constraints on the deviation from Newtonian gravity. This is because $p^{(3)}$ consists only of Fourier-phase informations and thus their constraints have good complementarity with those from $P(k)$, which is defined as the square of the Fourier amplitudes.

A. Linear bias model with $b_2 = 0$

Let us consider first linear bias model [$b_2 = 0$ in Eq. (2)]. Figure 3 plots the bispectra $B, Q, p^{(3)}$ in real space (left panels) and in redshift space (right panels) for $L_{\text{box}} = 500h^{-1}\text{Mpc}$ simulations. The survey volume is set to be $(L_{\text{box}})^3$ in Eq. (46). The bispectra at small φ are dominated by various nonlinear effects, whereas there are substantial uncertainties at large φ because of the small number of Fourier modes sampled. Given those, the agreement between predictions from perturbation theory (dashed lines) and N -body simulation data (solid circles with error-bar) is very satisfactory.

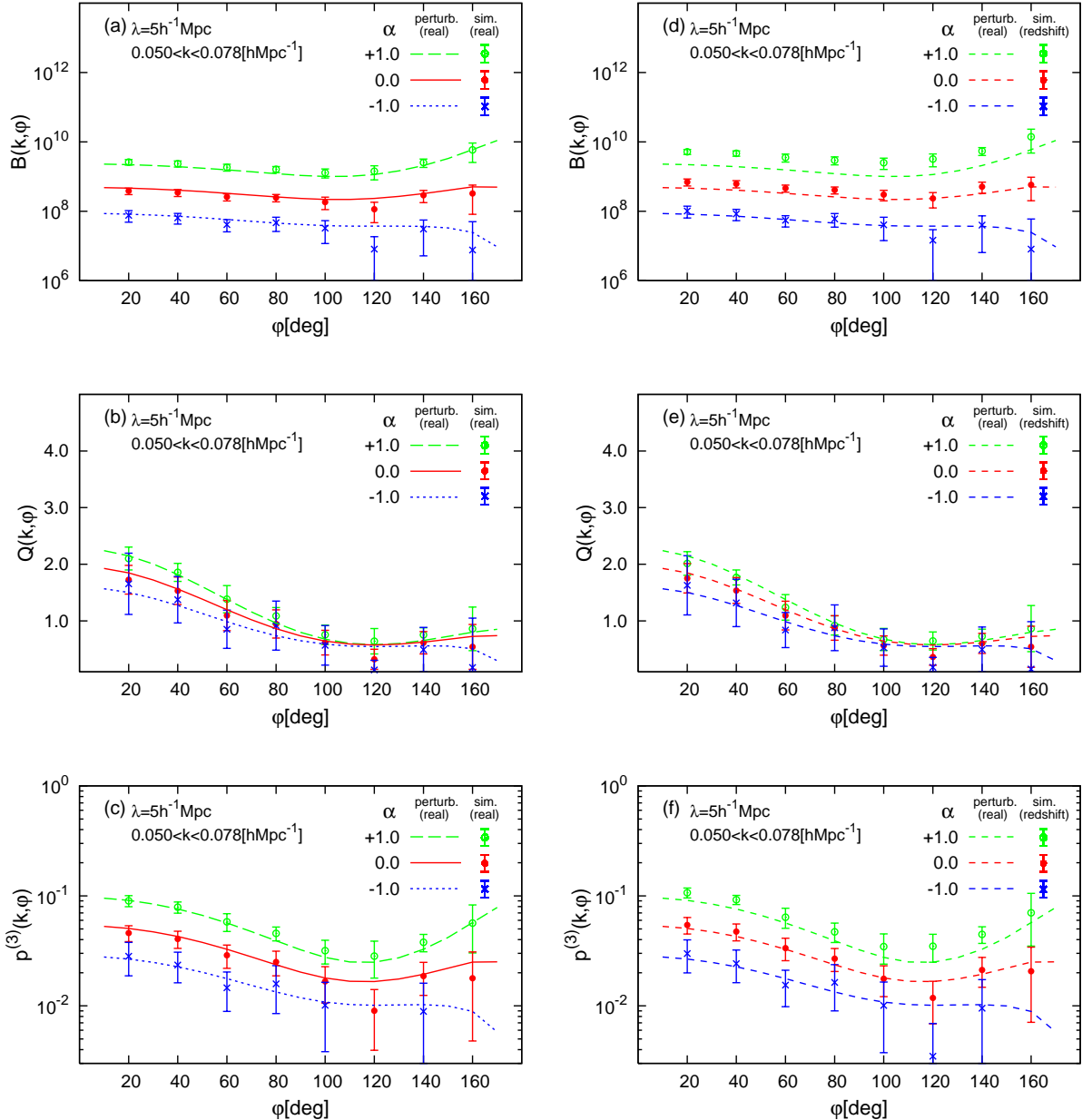


FIG. 3: Bispectra $B(k)$, $Q(k)$, and $p^{(3)}(k)$ from top to bottom as a function of φ measured in real space (left panels) and in redshift space (right panels). The range of $k \equiv |\mathbf{k}_1| = |\mathbf{k}_2|$ is indicated in each panel. The value of λ is fixed as $5h^{-1}\text{Mpc}$. The dashed, solid, dotted lines show the perturbation predictions in real space for $\alpha = +1.0$, 0.0 (Newtonian) and -1.0 , respectively. Symbols with error-bars show the results of simulations. Open circle, filled circle, cross symbol also mean $\alpha = +1.0$, 0.0 (Newton) and -1.0 , respectively.

The right panels of Fig. 3 shows the bispectra in redshift space. There, the results from our mock samples are shown by symbols with error bars. For comparison, we also show the results from perturbation theory in *real space*. In Fig. 3(d), Kaiser effect is clearly seen as an enhance at small φ .

We further examine the dependence of the bispectra on λ . Figure 4 compares the bispectra for different values of

λ . We have set $\alpha = 0.5$ (left panels) and $\alpha = -0.5$ (right panels).

Figure 5 shows $p^{(3)}(k)$ for the volume-limited SDSS catalogue and for our mock samples at k in the range of $0.072h\text{Mpc}^{-1} < k < 0.103h\text{Mpc}^{-1}$. They have a very similar shape, but their amplitude depends systematically on the value of α , the degree of deviations from the Newtonian case.

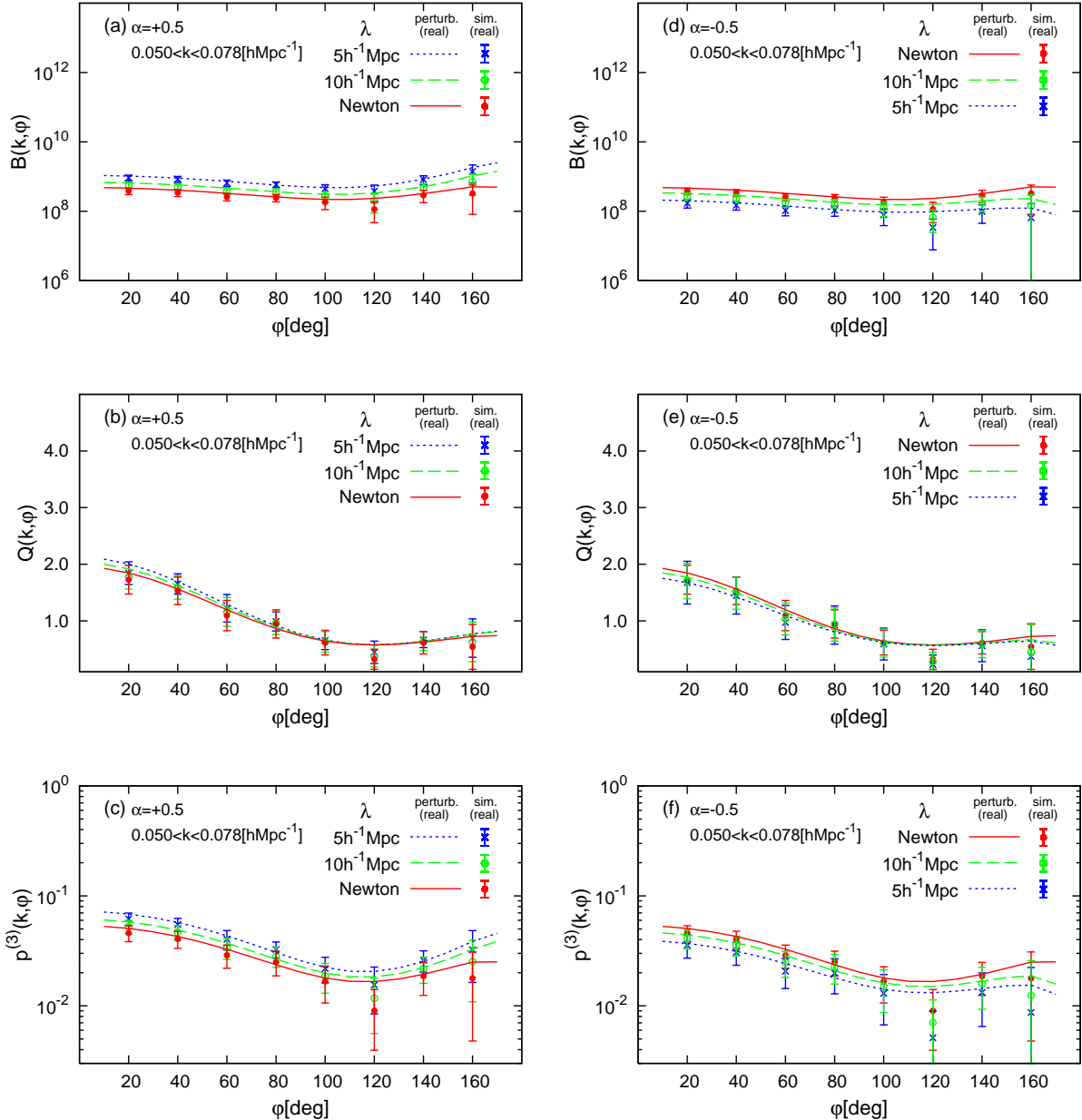


FIG. 4: Bispectra $B(k)$, $Q(k)$, and $p^{(3)}(k)$ from top to bottom as a function of φ measured in real space; *right*: $\alpha = 0.5$, *left*: $\alpha = -0.5$. The dotted, dashed, and solid lines show the perturbation predictions in real space for $\lambda = 5h^{-1}\text{Mpc}$, $\lambda = 10h^{-1}\text{Mpc}$, and $\lambda = \infty$ (Newtonian), respectively, while symbols indicate the corresponding simulation results.

Figure 6 plots constraints on the (α, λ) plane derived from the $\Delta\chi^2$ fit to the SDSS bispectrum using $p^{(3)}$ and assuming a linear bias ($b_2 = 0$). The constraints from the bispectrum are fairly consistent with, but slightly more stringent than, those from the power spectrum, which indicates the complementary role of the higher-order clustering statistics.

B. The effect of non-linear biasing

In reality, however, it may be more appropriate to analyze the higher-order clustering statistics adopting a non-linear bias model. In the case of the bispectrum, it implies to introduce the quadratic biasing parameter b_2 [see Eq. (2)]. In this bias model, the relation of $p_g^{(3)}$ for galax-

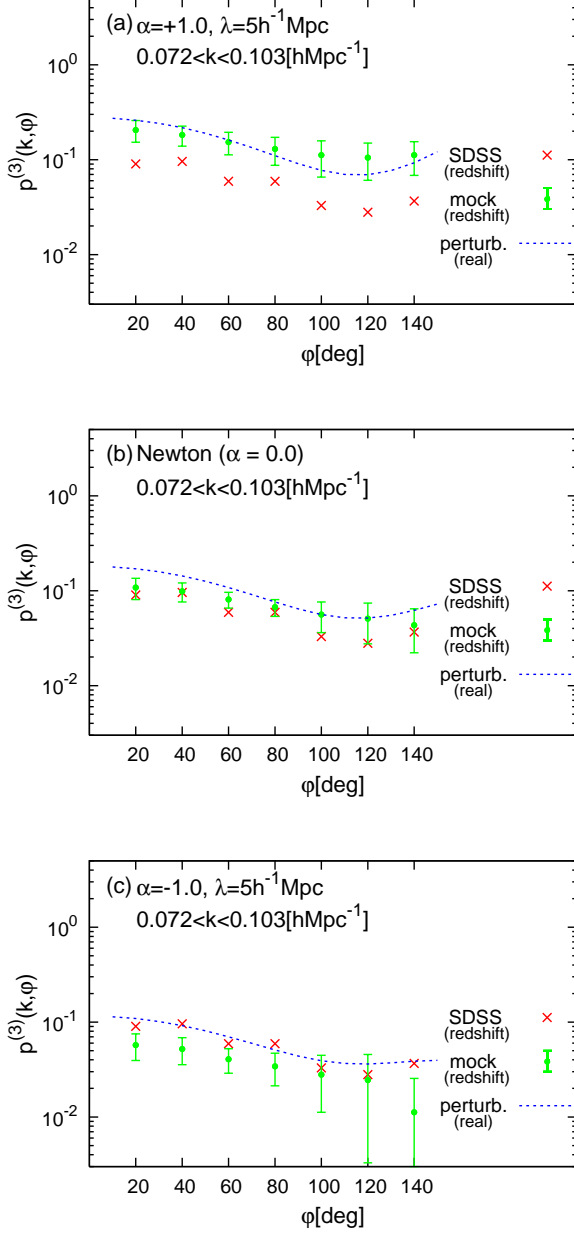


FIG. 5: Bispectra $p^{(3)}$ for SDSS galaxies (crosses), mock galaxy samples (solid circles with error bars), and perturbation theory predictions in real space (dotted line): (a) $\alpha = +1.0$ and $\lambda = 5h^{-1}\text{Mpc}$, (b) $\alpha = 0.0$ (Newtonian), (c) $\alpha = -1.0$ and $\lambda = 5h^{-1}\text{Mpc}$.

ies and $p^{(3)}$ for mass reduces to

$$p_g^{(3)}(\mathbf{k}_1, \mathbf{k}_2) = p^{(3)}(\mathbf{k}_1, \mathbf{k}_2) + \frac{b_2}{b_1} f(P_1, P_2, P_3), \quad (48)$$

$$f(P_1, P_2, P_3) \equiv \frac{P_1 P_2 + P_2 P_3 + P_3 P_1}{\sqrt{V_{\text{samp}} P_1 P_2 P_3}}, \quad (49)$$

where $P_i = P(k_i)$ for $i = 1, 2, 3$ [36].

Previous papers [36, 42] suggest that a simple linear

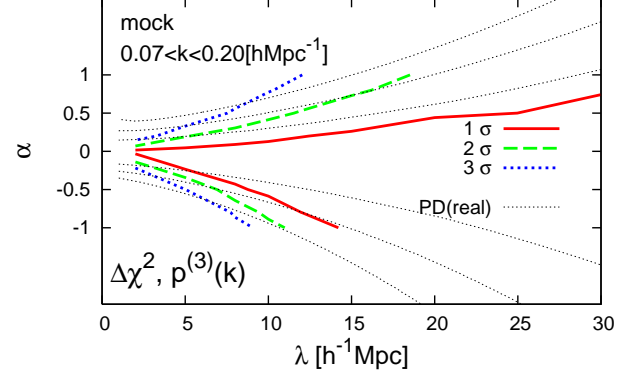


FIG. 6: Constraints on the $\alpha - \lambda$ plane from the $p^{(3)}$ analysis assuming $b_2 = 0$. The range of k is from 0.07 to 0.20 $h\text{Mpc}^{-1}$. Solid, dashed, thick dotted lines indicate 1σ , 2σ and 3σ confidence levels. Thin dotted lines are the same as those in Fig. 2(a).

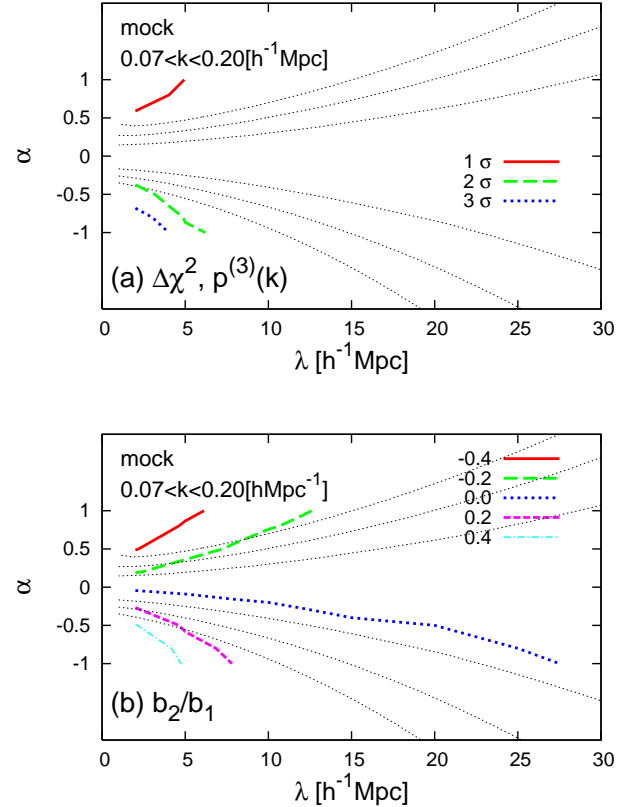


FIG. 7: (a) Constraints on α and λ from the $p^{(3)}$ analysis treating b_2/b_1 as a free parameter. (b) The best fit values of b_2/b_1 that gives minimum χ^2 for $p^{(3)}$. Thin dotted lines are the same as those in Fig. 2(a).

bias model in the Newtonian gravity model describes well the clustering of the volume-limited sample of SDSS galaxies, i.e., $b_2 \sim 0$ and $b_1 \sim 1$. We now repeat the similar analysis in the modified Newtonian model.

Figure 7(a) indicates constraints on the (α, λ) plane by treating b_2/b_1 as a free parameter, which should be compared with Figure 6 for $b_2 = 0$. The regions below the contours are excluded with the corresponding confidence level. Naturally the bispectrum alone does not constrain (α, λ) significantly in this generalized model. While the $\alpha = 0$ models are excluded with a 1σ confidence level, the conclusion is not statistically significant. In turn, however, we can derive constraints on the value of b_2/b_1 for the modified gravity model by combining the constraints from power spectrum (independent of the value of b_2/b_1). Figure 7(b) shows the contours of the best-fit value of b_2/b_1 that gives the minimum χ^2 for $p^{(3)}(k)$ on the plane. Figure 7(b) suggests that b_2/b_1 should satisfy $-0.4 < b_2/b_1 < 0.3$, which is the first constraint on the quadratic biasing parameter in the modified Newtonian model.

VIII. SUMMARY

We have derived constraints on possible deviations from Newtonian gravity using the power spectrum and the bispectrum of Sloan Digital Sky Survey galaxies. Our model assumes an additional Yukawa-like term with two parameters that characterize the amplitude, α , and the length scale, λ , of the modified gravity. We have predicted the power spectrum and the bispectrum using two different methods, the perturbation theory and direct N -body simulations, and found the good agreement in real space as long as the biasing between galaxies and mass is neglected. In order to take the biasing effect into consideration, we adopt a quadratic biasing model. By comparing with the mock catalogues constructed from our simulations, we have derived constraints on α and λ .

This method allows us to compute the clustering statistics in redshift space and taking account of various observational effects such as survey geometry as well. The resulting constraints from power spectrum are consistent with those obtained in our earlier work, indicating the validity of the previous empirical modeling of gravitational nonlinearity in the modified Newtonian model. If linear biasing is adopted, the bispectrum of the SDSS galaxies yields constraints very similar to those from the power spectrum. If we allow for the nonlinear biasing instead, we find that the ratio of the quadratic to linear biasing coefficients, b_2/b_1 , should satisfy $-0.4 < b_2/b_1 < 0.3$ in the modified Newtonian model.

Future observations will exploit large ground-based telescopes to probe the matter density distribution by weak gravitational lensing. Combined with data from galaxy redshift surveys, lensing observations will provide invaluable informations on galaxy bias. Then it will be possible to put more stringent constraints on deviations from Newton's law of gravity at cosmological scales, using the methodology presented in the this paper.

Acknowledgements

We would like to thank Atsushi Taruya, Kazuhiro Yahata, Takahiro Nishimichi, Shun Saito, and Issya Kayo for useful discussions and comments. A. S. acknowledge the support from Grants-in-Aid for Japan Society for the Promotion of Science Fellows. The simulations were performed at the Data-Reservoir at the University of Tokyo. We thank Mary Inaba and Kei Hiraki at the University of Tokyo for providing the computational resources. This work is supported in part by Grants-in-Aid for Scientific research of the Ministry of Education, Culture, Sports, Science and Technology (No. 17684008, and 18072002), and by JSPS (Japan Society for Promotion of Science) Core-to-Core Program "International Research Network for Dark Energy".

-
- [1] D. N. Spergel *et al.*, astro-ph/0603449.
 - [2] C. L. Bennett *et al.*, *Astrophys. J. Suppl.* **148**, 1 (2003)
 - [3] D. N. Spergel *et al.* *Astrophys. J. Suppl.* **148**, 175 (2003)
 - [4] M. Tegmark *et al.* *Astrophys. J.* **606**, 702 (2004)
 - [5] S. Cole *et al.* *Mon. Not. Roy. Astron. Soc.* **362**, 505 (2005)
 - [6] R. A. Knop *et al.*, *Astrophys. J.* **598**, 102 (2003)
 - [7] P. Astier *et al.*, *A&A*, **447**, 31 (2006)
 - [8] A. G. Riess *et al.*, astro-ph/0611572
 - [9] G. R. Dvali, G. Gabadadze and M. Porrati, *Phys. Lett. B* **485**, 208 (2000)
 - [10] C. Deffayet, *Phys. Lett. B* **502**, 199 (2001)
 - [11] R. H. Sanders and S. S. McGaugh, *Ann. Rev. Astron. Astrophys.* **40**, 263 (2002)
 - [12] R. Scarpa, in *AIP Conference Proceedings, Vol 822, 2006*, edited by E.J Lerner and J.B. Almeida, p. 253.
 - [13] J. D. Bekenstein, *Phys. Rev. D* **70**, 083509 (2004); *D* **71**, 069901(E) (2005)
 - [14] N. Arkani-Hamed, H. C. Cheng, M. A. Luty and S. Mukohyama, *JHEP* **0405**, 074 (2004)
 - [15] N. Arkani-Hamed, P. Creminelli, S. Mukohyama and M. Zaldarriaga, *JCAP* **0404**, 001 (2004)
 - [16] E. Fischbach and C. L. Talmadge, *The search for non-Newtonian gravity* (Springer, New York, 1999)
 - [17] E. G. Adelberger, B. R. Heckel and A. E. Nelson, *Ann. Rev. Nucl. Part. Sci.* **53**, 77 (2003)
 - [18] C. D. Hoyle, D. J. Kapner, B. R. Heckel, E. G. Adelberger, J. H. Gundlach, U. Schmidt and H. E. Swanson, *Phys. Rev. D* **70**, 042004 (2004)
 - [19] J. A. Frieman and B. Gradwohl, *Phys. Rev. Lett.* **67**, 2926 (1991).
 - [20] A. Shirata, T. Shiromizu, N. Yoshida and Y. Suto, *Phys. Rev. D* **71**, 064030 (2005)
 - [21] C. Sealton, L. Verde and R. Jimenez, *Phys. Rev. D* **71**, 083004 (2005)

- [22] C. Deffayet, G. R. Dvali and G. Gabadadze, Phys. Rev. D **65**, 044023 (2002)
- [23] A. Lue, R. Scoccimarro and G. D. Starkman, Phys. Rev. D **69**, 124015 (2004)
- [24] J. S. Alcaniz and N. Pires, Phys. Rev. D **70**, 047303 (2004)
- [25] A. Lue and G. D. Starkman, Phys. Rev. D **70**, 101501 (2004)
- [26] K. Yamamoto, B. A. Bassett, R. C. Nichol, Y. Suto and K. Yahata, Phys. Rev. D **74**, 063525 (2006)
- [27] D. J. Eisenstein and W. Hu, Astrophys. J. **496**, 605 (1998)
- [28] J. A. Peacock and S. J. Dodds, Mon. Not. Roy. Astron. Soc. **280**, L19 (1996)
- [29] R. Juszkiewicz, Mon. Not. Roy. Astron. Soc. **197**, 931 (1981)
- [30] E. T. Vishniac Mon. Not. Roy. Astron. Soc. **203**, 345 (1983)
- [31] Y. Suto and M. Sasaki, Phys. Rev. Lett. **66**, 264 (1991).
- [32] N. Makino, M. Sasaki and Y. Suto, Phys. Rev. D **46**, 585 (1992).
- [33] F. Bernardeau, arXiv:astro-ph/0409224.
- [34] P. Bode and J. P. Ostriker, Astrophys. J. Suppl. **145**, 1 (2003)
- [35] G. Efstathiou, M. Davis, C. S. Frenk and S. D. M. White, Astrophys. J. Suppl. **57**, 241 (1985).
- [36] C. Hikage, T. Matsubara, Y. Suto, C. Park, A. S. Szalay and J. Brinkmann, Publ. Astron. Soc. Jap. **57**, 709 (2005)
- [37] H.A. Feldman, N. Kaiser, and J.A. Peacock, Astrophys. J. **426** 23 (1994)
- [38] H. F. Stabenau and B. Jain, arXiv:astro-ph/0604038.
- [39] H. Magira, Y. P. Jing and Y. Suto, Astrophys. J. **528**, 30 (2000)
- [40] T. Matsubara, Astrophys. J. **591**, L79 (2003)
- [41] C. Hikage, T. Matsubara and Y. Suto, Astrophys. J. **600**, 553 (2004)
- [42] T. Nishimichi *et al.*, Publ. Astron. Soc. Jap. **59**, 93 (2007)